

## Supporting Information

# Facile Surface Reconstructions of Cobalt–Copper Phosphide Heterostructures Enable Efficient Electrocatalytic Glycerol Oxidation for Energy-Saving Hydrogen Evolution

Zhengzhe Xie,<sup>†[a](#)</sup> Kang Wang,<sup>†[b](#)</sup> Yu Zou,<sup>a</sup> Guobing Ying,<sup>\*[b](#)</sup> and Jiang Jiang<sup>\*[a](#)</sup>

<sup>a</sup>*i*-Lab, CAS Key Laboratory of Nano-Bio Interface, Suzhou Institute of Nano-Tech and Nano-Bionics, Chinese Academy of Sciences, Suzhou 215123, China

<sup>b</sup>Department of Materials Science and Engineering, College of Mechanics and Materials, Hohai University, Nanjing 211100, China

<sup>†</sup>These authors contributed equally

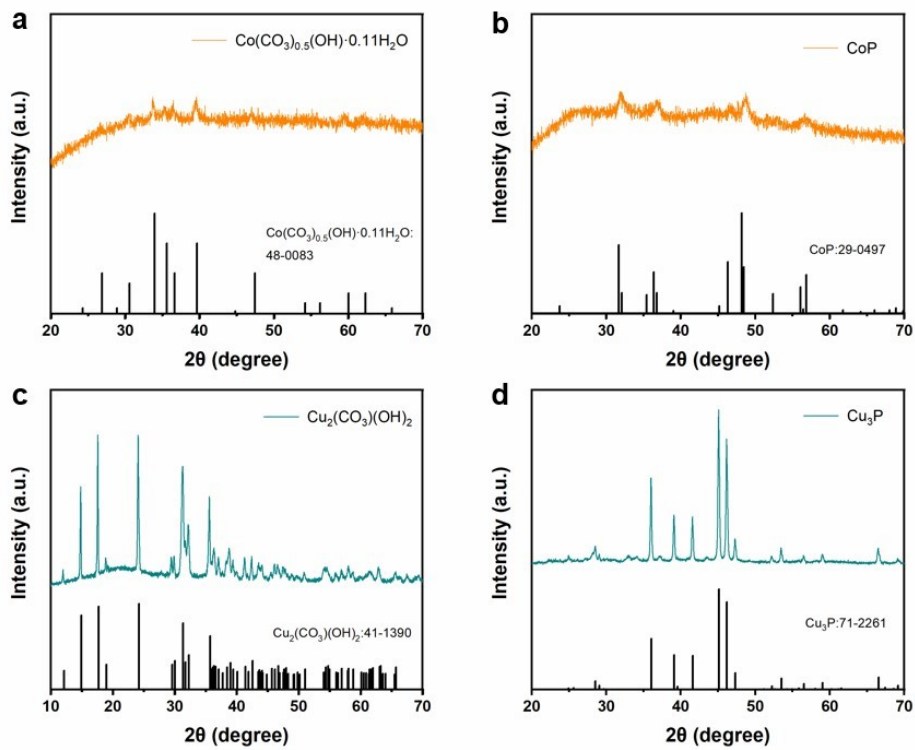


**Fig. S1** XRD patterns of (a)  $\text{Co}(\text{CO}_3)_{0.5}(\text{OH}) \cdot 0.11\text{H}_2\text{O}$ , (b) CoP, (c)  $\text{Cu}_2(\text{CO}_3)(\text{OH})_2$ , and (d)  $\text{Cu}_3\text{P}$ .

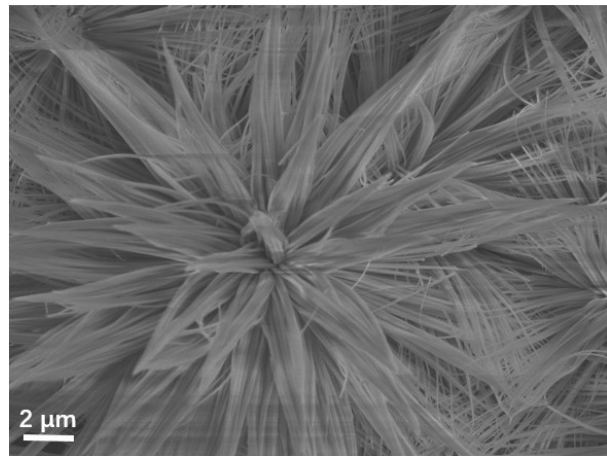


**Fig. S2** SEM image of  $(\text{Co,Cu})_2\text{CO}_3(\text{OH})_2$ .

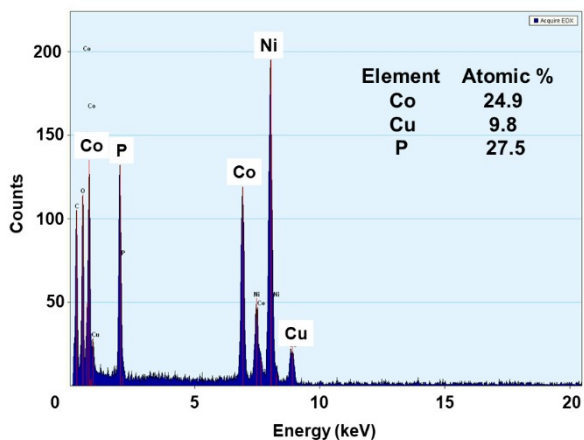


**Fig. S3** EDS analysis and elemental quantification of CoP-Cu<sub>3</sub>P.

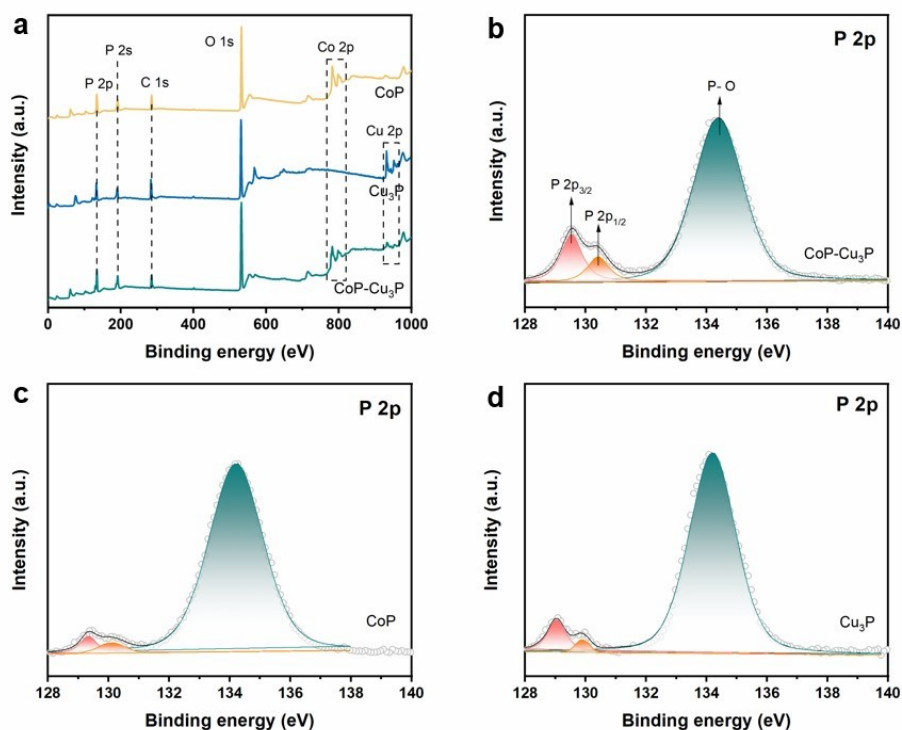


**Fig. S4** (a) XPS survey scans of CoP, Cu<sub>3</sub>P, and CoP-Cu<sub>3</sub>P in the binding energy range of 0-1000 eV. High resolution P 2p XPS spectra of (b) CoP-Cu<sub>3</sub>P, (c) CoP, and (d) Cu<sub>3</sub>P.

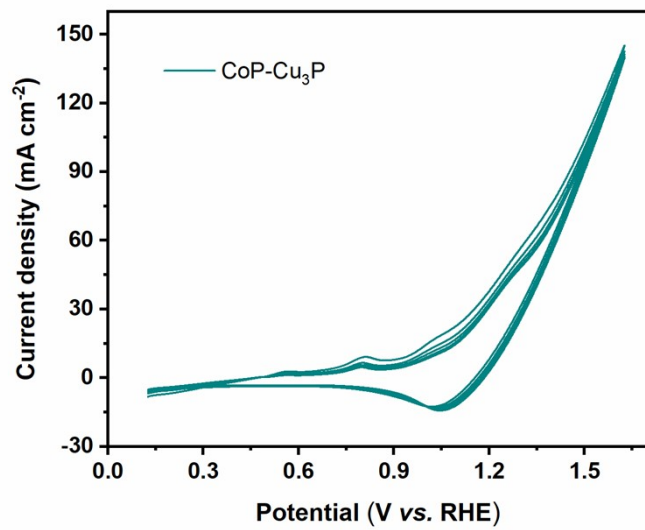


**Fig. S5** CV curves in the potential range of 0.1-1.6 V versus RHE for CoP-Cu<sub>3</sub>P, with a scan rate of 5 mV s<sup>-1</sup>.

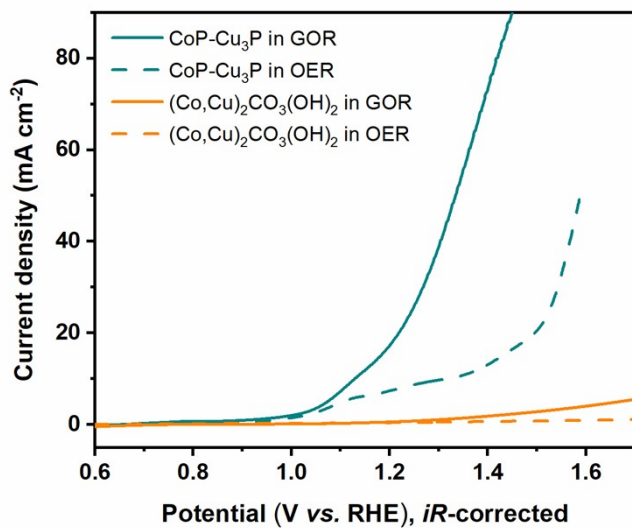


**Fig. S6** LSV curves of CoP-Cu<sub>3</sub>P and (Co,Cu)<sub>2</sub>CO<sub>3</sub>(OH)<sub>2</sub> grown on carbon cloth in 1 M KOH solution with (solid lines) and without (dashed lines) 0.1 M glycerol addition.

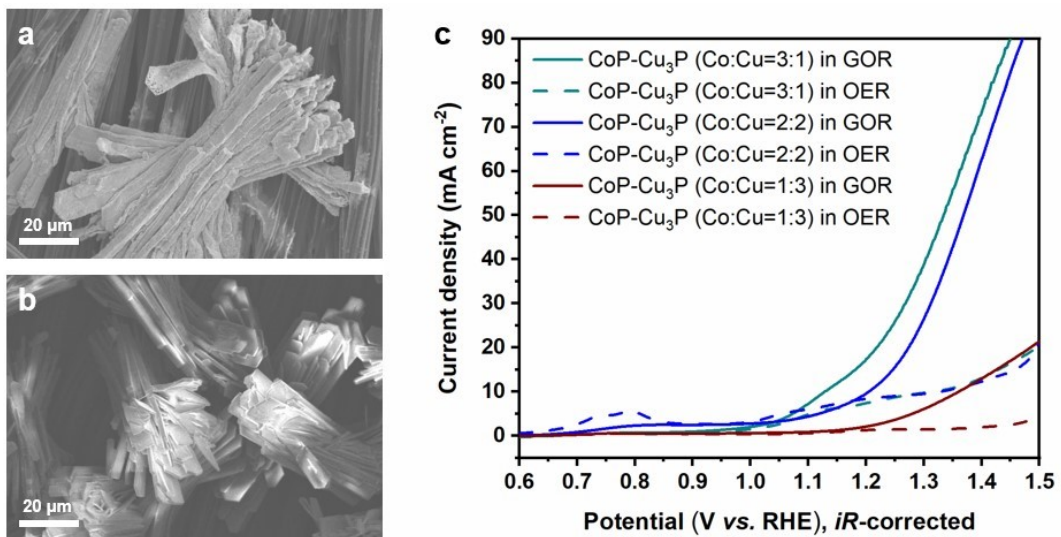


**Fig. S7** SEM images of CoP-Cu<sub>3</sub>P composites with different initial feeding Co:Cu ratio, (a) Co:Cu=2:2, (b) Co:Cu=1:3. (c) LSV curves of CoP-Cu<sub>3</sub>P/CC with different Co:Cu ratio in CoP-Cu<sub>3</sub>P composites, in 1 M KOH solution with (solid lines) and without (dashed lines) 0.1 M glycerol addition.

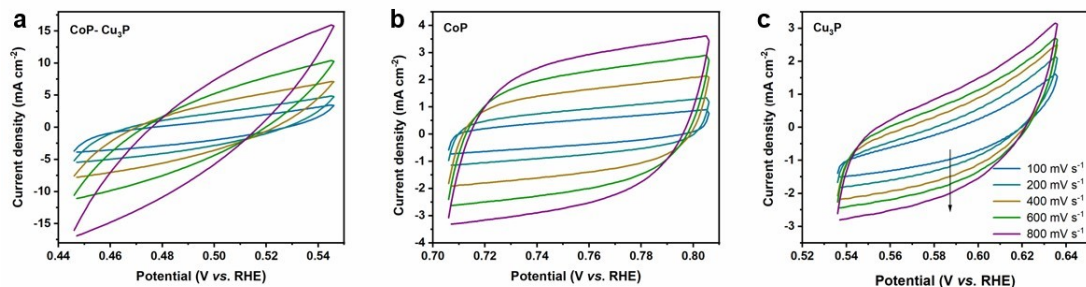


**Fig. S8** Electrochemical capacitance measurements for various electrodes. CV were taken in a potential range with no Faradic processes for (a) CoP-Cu<sub>3</sub>P, (b) CoP, and (c) Cu<sub>3</sub>P.

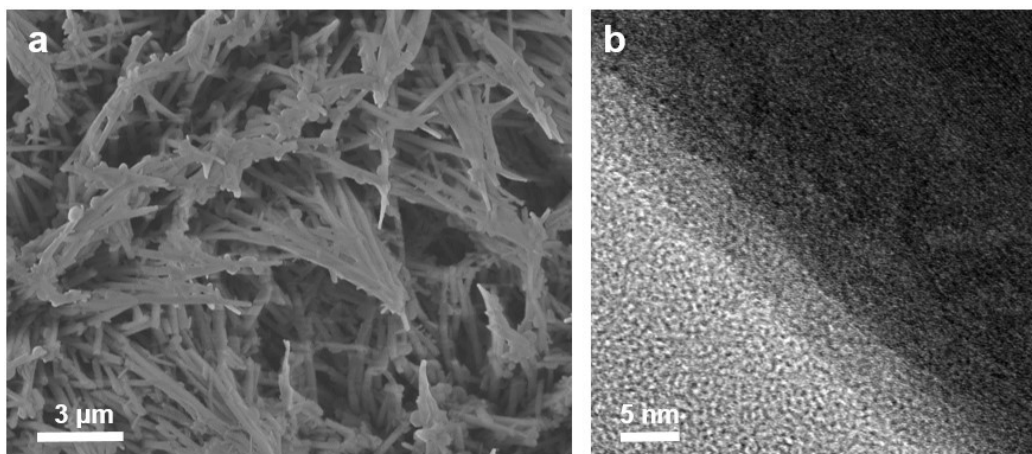


**Fig. S9** (a) SEM and (b) TEM images of CoP-Cu<sub>3</sub>P after GOR process.

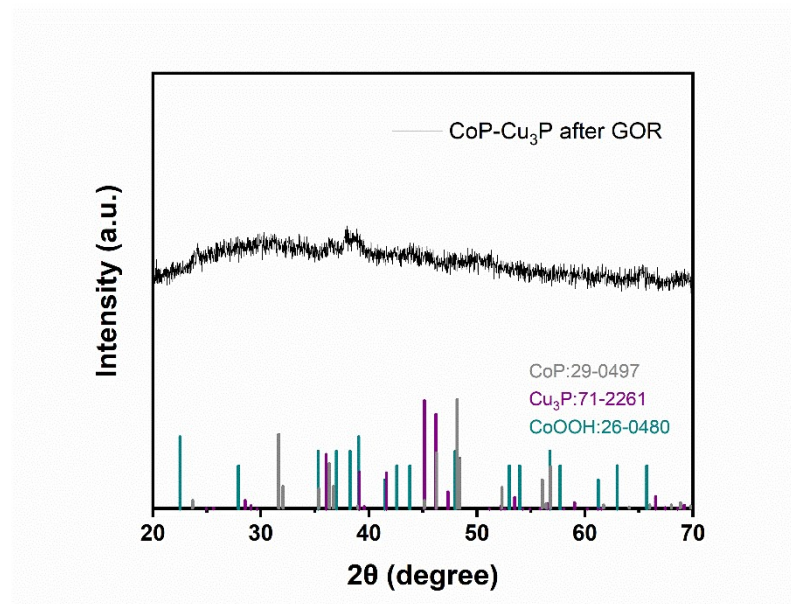


**Fig. S10** XRD pattern of CoP-Cu<sub>3</sub>P after GOR process.

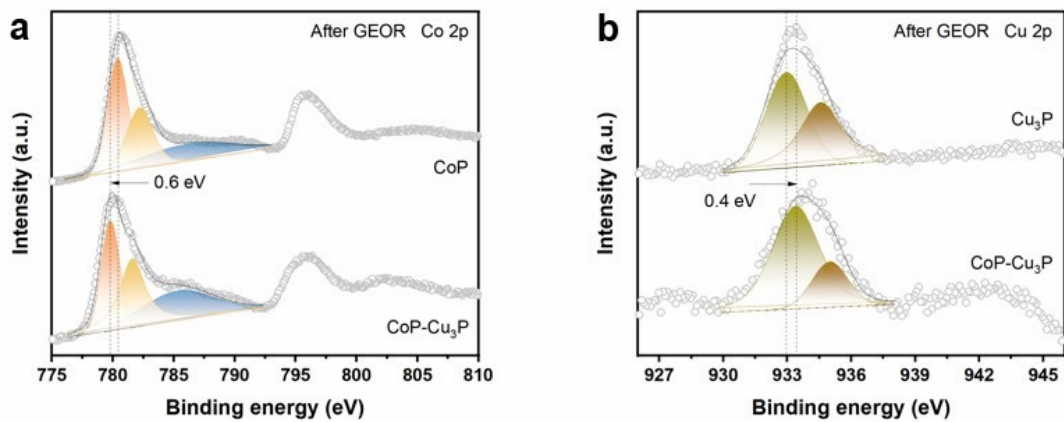


**Fig. S11** (a) High resolution Co 2p XPS spectra of CoP and CoP-Cu<sub>3</sub>P after GOR process. (b) High resolution Cu 2p XPS spectra of Cu<sub>3</sub>P and CoP-Cu<sub>3</sub>P after GOR process.

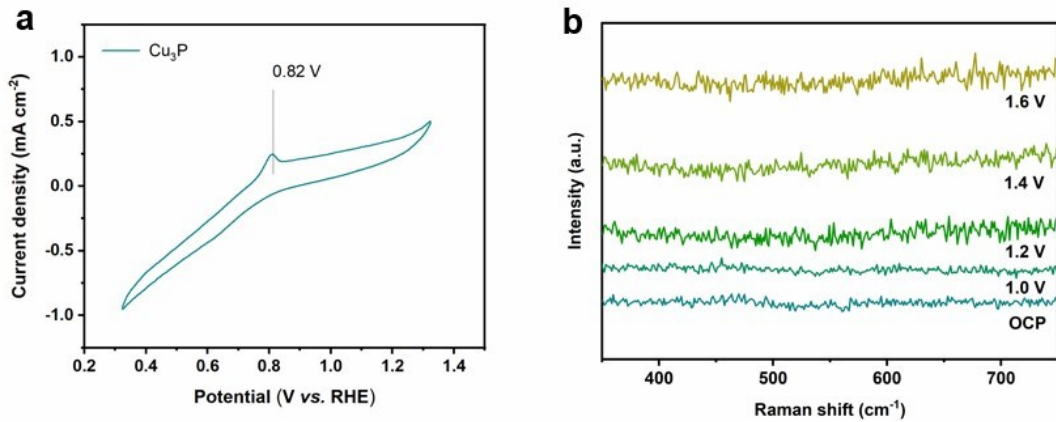


**Fig. S12** (a) CV curve in the potential range of 0.3-1.3 V versus RHE for  $\text{Cu}_3\text{P}$ , with a scan rate of  $5 \text{ mV s}^{-1}$ . (b) In situ Raman spectra recorded on  $\text{Cu}_3\text{P}$  electrode at increasing applied potentials from OCP to 1.6 V.

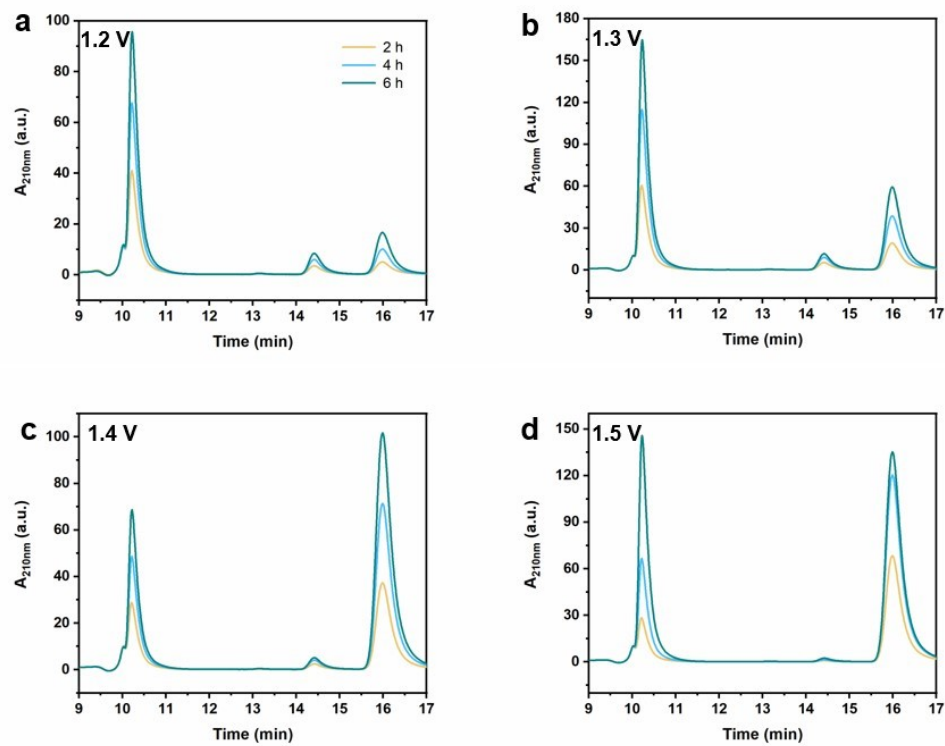


**Fig. S13** HPLC chromatograms of collected solution products after GOR on CoP- $\text{Cu}_3\text{P}$  at a constant potential of (a) 1.2 V, (b) 1.3 V, (c) 1.4 V, and (d) 1.5 V vs. RHE in 1 M KOH containing 0.1 M glycerol.

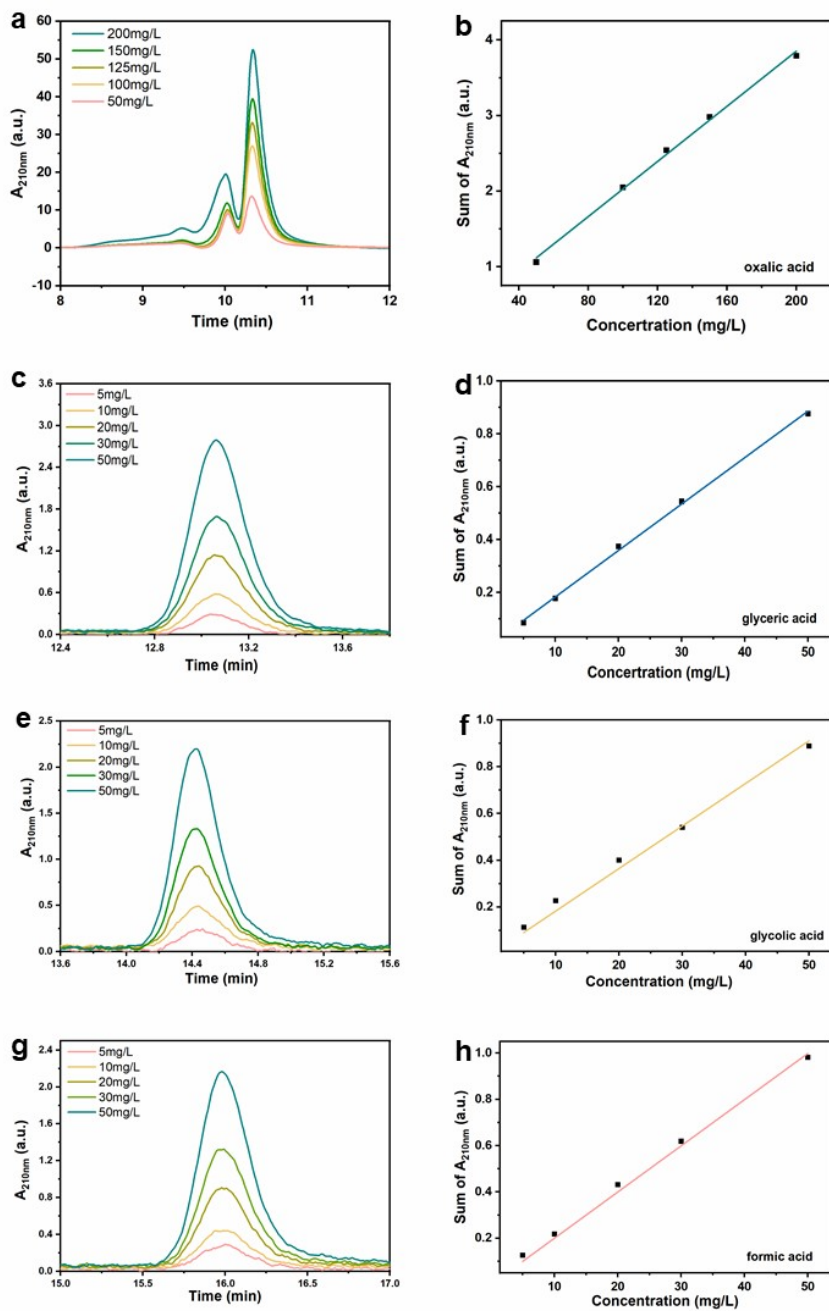


**Fig. S14** The HPLC chromatograms of standard chemicals with known concentrations (left column) and the obtained calibration curves (right column): (a, b) oxalic acid, (c, d) glyceric acid, (e, f) glycolic acid, and (g, h) formic acid.

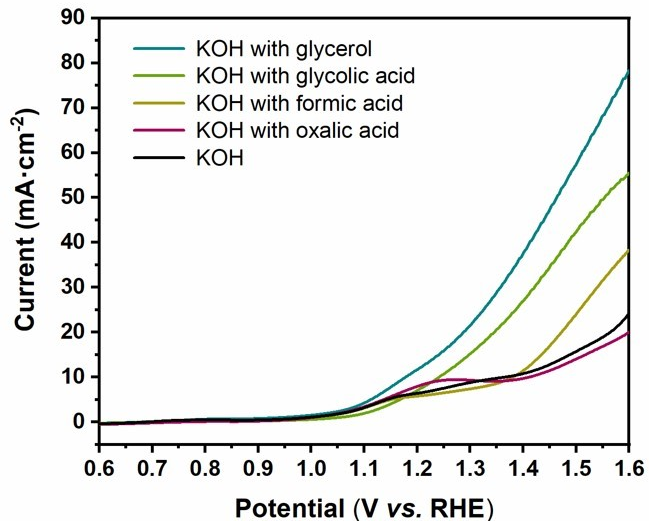


**Fig. S15** LSV curves of CoP-Cu<sub>3</sub>P/CC in 1 M KOH solution with GOR intermediate products (oxalic acid, glycolic acid, and formic acid).

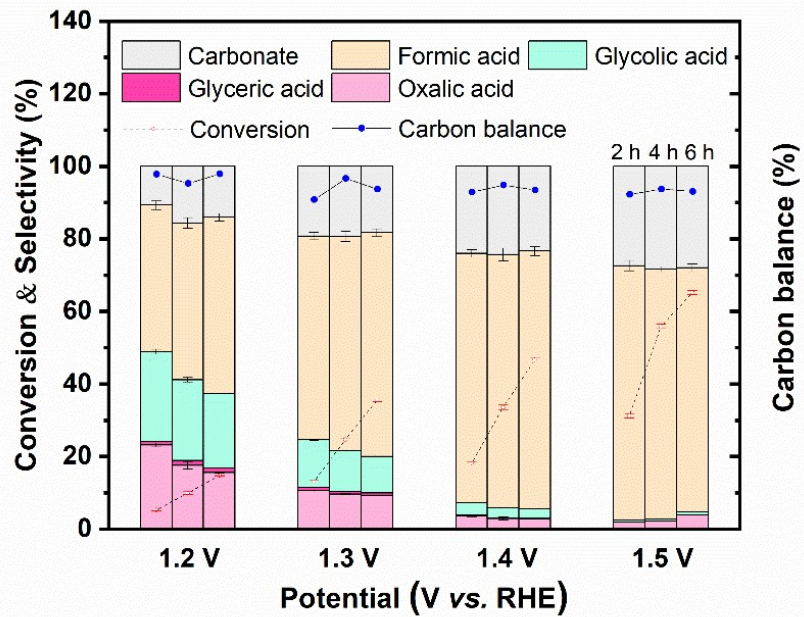


**Fig. S16** The glycerol conversion, oxidation products selectivity, and carbon balance at different time points and applied potentials (1 M KOH, 0.1 M glycerol).

The glycerol conversion, selectivity of the product and carbon balance are calculated by the following equations:

$$\text{Glycerol conversion} = \frac{n_{\text{converted glycerol}}}{n_{\text{initial glycerol}}} \times 100\%$$

$$Selectivity_{product} = \frac{n_{product}}{n_{total}} \times 100\%$$

$$Carbon\ balance = \frac{3n_{C3} + 2n_{C2} + n_{C1} + 3n_{final\ glycerol}}{3n_{initial\ glycerol}} \times 100\%$$

where  $n_{product}$  indicates the moles of the product,  $n_{total}$  denotes the moles of the total product,  $n_{initial}$  glycerol,  $n_{converted}$  glycerol, and  $n_{final}$  glycerol are the initial, converted, and final moles of glycerol,  $n_{C1}$ ,  $n_{C2}$ , and  $n_{C3}$  are the moles of C1, C2, and C3 products, respectively.

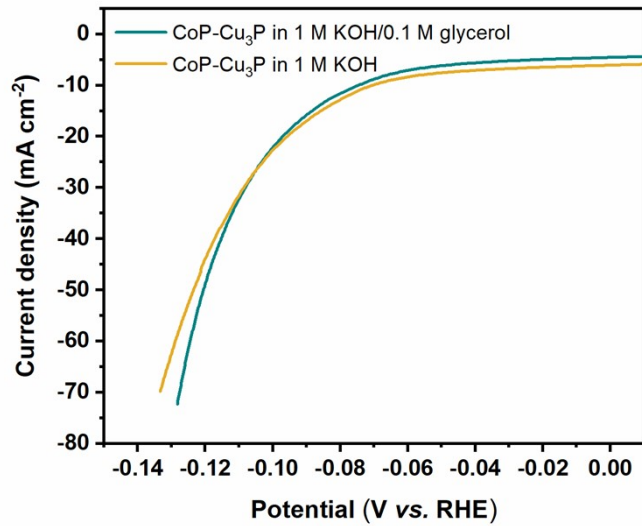


**Fig. S17** LSV curves of CoP-Cu<sub>3</sub>P/CC in 1 M KOH solution with (cyan) and without (yellow) 0.1 M glycerol addition.

**Table S1.** Comparison of the GOR acitivity between CoP-Cu<sub>3</sub>P/CC and some other electrocatalysts in the recent literature reports.

Anodic catalyst	Electrolyte	Applied potential at 10 mA cm <sup>-2</sup> (V)	Ref.
CoP-Cu <sub>3</sub> P/CC	1 M KOH + 0.1 M glycerol	1.13	This work
CuCo <sub>2</sub> O <sub>4</sub>	0.1 M KOH + 0.1 M glycerol	1.30	[1]
CuCo-oxide	0.1 M KOH + 0.1 M glycerol	1.25	[2]
(Cu <sub>1-x</sub> Co <sub>x</sub> ) <sub>2</sub> CO <sub>3</sub> (OH) <sub>2</sub>	1 M KOH + 0.1 M glycerol	>1.4	[3]
NiO <sub>x</sub> /MWCNTs	1 M KOH + 1 M glycerol	1.31	[4]
Ni-Mo-N/CFC	1 M KOH + 0.1 M glycerol	1.30	[5]
Ni-Mo-N/NF	1 M KOH + 0.1 M glycerol	1.16	[6]
CoMoO <sub>4</sub>	1 M KOH + 0.1 M glycerol	1.239	[7]
HEA-CoNiCuMnMo	1 M KOH + 0.1 M glycerol	1.25	[8]
CoNi hydroxide	1 M KOH + 0.1 M glycerol	1.35 V @100 mA cm <sup>-2</sup>	[9]
NiV LDH	1 M KOH + 0.1 M glycerol	1.23	[10]

**Table S2.** Comparison of the chemical-assisted hydrogen evolution reaction performance between the CoP-Cu<sub>3</sub>P/CC||CoP-Cu<sub>3</sub>P/CC and some other reported systems.

Anodic catalyst	Cathodic catalyst	Electrolyte	Cell voltage at 10 mA cm <sup>-2</sup> (V)	Ref.
CoP-Cu <sub>3</sub> P/CC	CoP-Cu <sub>3</sub> P/CC	1 M KOH + 0.1 M glycerol	1.21	This work
Ni-Mo-N/CFC	Ni-Mo-N/CFC	1 M KOH + 0.1 M glycerol	1.36	[5]
NC/Ni-Mo-N/NF	NC/Ni-Mo-N/NF	1 M KOH + 0.1 M glycerol	1.38	[6]
HEA-CoNiCuMnMo	RhIr/Ti	1 M KOH + 0.1 M glycerol  0.5 M H <sub>2</sub> SO <sub>4</sub>	0.55	[8]
NiV LDH	P-NiV LDH	1 M KOH + 0.1 M glycerol	1.25	[10]
Ni <sub>3</sub> N-Ni <sub>0.2</sub> Mo <sub>0.8</sub> N/CC	Ni <sub>3</sub> N-Ni <sub>0.2</sub> Mo <sub>0.8</sub> N/CC	1 M KOH + 0.1 M glycerol	1.40	[11]
MnO <sub>2</sub>	Pt/C	0.005 M H <sub>2</sub> SO <sub>4</sub> + 0.2 M glycerol	1.36	[12]
Ni <sub>2</sub> P-CoP/NF	Ni <sub>2</sub> P-CoP/NF	1 M KOH + 0.5 M methanol	1.3	[13]
Ni <sub>2</sub> P	F-β-FeOOH	1 M KOH + 0.33 M ethanol	1.46	[14]
Co-S-P/CC	Co-S-P/CC	1 M KOH + 1 M ethanol	1.63	[15]
NiFeO <sub>x</sub> -NF	NiFeN <sub>x</sub> -NF	1 M KOH + 0.1 M glucose	1.39 @100 mA cm <sup>-2</sup>	[16]
Co-Ni alloy	Co-Ni alloy	1 M KOH + 0.1 M glucose	1.39	[17]
NiS@Ni <sub>3</sub> S <sub>2</sub> /NiMoO <sub>4</sub>	NiS@Ni <sub>3</sub> S <sub>2</sub> /NiMoO <sub>4</sub>	1 M KOH + 0.5 M urea	1.40	[18]
CoS <sub>2</sub> NA/Ti	CoS <sub>2</sub> NA/Ti	1 M KOH + 0.3 M urea	1.59	[19]

## References:

- [1] Han, X.; Sheng, H.; Yu, C.; Walker, T. W.; Huber, G. W.; Qiu, J.; Jin, S., *ACS Catal.* 2020, 10, 6741-6752.
- [2] Oh, L. S.; Park, M.; Park, Y. S.; Kim, Y.; Yoon, W.; Hwang, J.; Lim, E.; Park, J. H.; Choi, S. M.; Seo, M. H.; Kim, W. B.; Kim, H. J., *Adv. Mater.* 2022, e2203285.
- [3] Braun, M.; Behrendt, G.; Krebs, M. L.; Dimitri, P.; Kumar, P.; Sanjuán, I.; Cychy, S.; Brix, A. C.; Morales, D. M.; Hörlöck, J.; Hartke, B.; Muhler, M.; Schuhmann, W.; Behrens, M.; Andronescu, C., *ChemElectroChem* 2022, 9, e202200267.
- [4] Morales, D. M.; Jambrec, D.; Kazakova, M. A.; Braun, M.; Sikdar, N.; Koul, A.; Brix, A. C.; Seisel, S.; Andronescu, C.; Schuhmann, W., *ACS Catal.* 2022, 982-992.
- [5] Li, Y.; Wei, X.; Chen, L.; Shi, J.; He, M., *Nat. Commun.* 2019, 10, 5335.

- [6] Xu, Y.; Liu, M.; Wang, S.; Ren, K.; Wang, M.; Wang, Z.; Li, X.; Wang, L.; Wang, H., *Appl. Catal., B* 2021, 298, 120493.
- [7] Yu, X.; Araujo, R. B.; Qiu, Z.; Campos dos Santos, E.; Anil, A.; Cornell, A.; Pettersson, L. G. M.; Johnsson, M., *Adv. Energy Mater.* 2022, 2103750.
- [8] Fan, L.; Ji, Y.; Wang, G.; Chen, J.; Chen, K.; Liu, X.; Wen, Z., *J. Am. Chem. Soc.* 2022, 144, 7224-7235.
- [9] He, Z.; Hwang, J.; Gong, Z.; Zhou, M.; Zhang, N.; Kang, X.; Han, J. W.; Chen, Y., *Nat. Commun.* 2022, 13, 3777.
- [10] Dong, L.; Chang, G.-R.; Feng, Y.; Yao, X.-Z.; Yu, X.-Y., *Rare Met.* 2022, 41, 1583-1594.
- [11] Liu, X.; Fang, Z.; Teng, X.; Niu, Y.; Gong, S.; Chen, W.; Meyer, T. J.; Chen, Z., *J. Energy Chem.* 2022, 72, 432-441.
- [12] Li, Y.; Wei, X.; Chen, L.; Shi, J., *Angew. Chem., Int. Ed.* 2021, 60, 21464-21472.
- [13] Wu, D.; Hao, J.; Wang, W.; Yu, Y.; Fu, X. Z.; Luo, J. L., *ChemSusChem* 2021, 14, 5450-5459.
- [14] Chen, G.-F.; Luo, Y.; Ding, L.-X.; Wang, H., *ACS Catal.* 2017, 8, 526-530.
- [15] Sheng, S.; Ye, K.; Sha, L.; Zhu, K.; Gao, Y.; Yan, J.; Wang, G.; Cao, D., *Inorg. Chem. Front.* 2020, 7, 4498-4506.
- [16] Liu, W. J.; Xu, Z.; Zhao, D.; Pan, X. Q.; Li, H. C.; Hu, X.; Fan, Z. Y.; Wang, W. K.; Zhao, G. H.; Jin, S.; Huber, G. W.; Yu, H. Q., *Nat. Commun.* 2020, 11, 265.
- [17] Lin, C.; Zhang, P.; Wang, S.; Zhou, Q.; Na, B.; Li, H.; Tian, J.; Zhang, Y.; Deng, C.; Meng, L.; Wu, J.; Liu, C.; Hu, J.; Zhang, L., *J. Alloys Compd.* 2020, 823, 153784.
- [18] Sha, L.; Liu, T.; Ye, K.; Zhu, K.; Yan, J.; Yin, J.; Wang, G.; Cao, D., *J. Mater. Chem. A* 2020, 8, 18055-18063.
- [19] S. Wei, X. Wang, J. Wang, X. Sun, L. Cui, W. Yang, Y. Zheng, J. Liu, *Electrochim. Acta* 2017, 246, 776-782.